Technical Report

484

W. D. Fitzgerald

Limited Electronic Scanning with a Near-Field Cassegrainian System

24 September 1971

Prepared for the Office of the Chief of Research and Development, Department of the Army, under Electronic Systems Division Contract F19628-70-C-0230 by

Lincoln Laboratory

MASSACHUSETTS INSTITUTE OF TECHNOLOGY

Lexington, Massachusetts

DOCUMENT CONTROL DATA - R&D

(Security classification of title, body of abstract and indexing annotation must be entered when the overall report is classified)

1. ORIGINATING ACTIVITY *(Corporate author)* Lincoln Laboratory, M.I.T.	2a. REPORT SECURITY CLASSIFICATION Unclassified 2b. GROUP None

3. REPORT TITLE

Limited Electronic Scanning with a Near-Field Cassegrainian System

4. DESCRIPTIVE NOTES *(Type of report and inclusive dates)*
Technical Report

5. AUTHOR(S) *(Last name, first name, initial)*

Fitzgerald, William D.

6. REPORT DATE	7a. TOTAL NO. OF PAGES	7b. NO. OF REFS
24 September 1971	28	14

8a. CONTRACT OR GRANT NO. F19628-70-C-0230 b. PROJECT NO. 7X263304D215 c. d.	9a. ORIGINATOR'S REPORT NUMBER(S) Technical Report 484 9b. OTHER REPORT NO(S) *(Any other numbers that may be assigned this report)* ESD-TR-71-271

10. AVAILABILITY/LIMITATION NOTICES

Approved for public release; distribution unlimited.

11. SUPPLEMENTARY NOTES	12. SPONSORING MILITARY ACTIVITY
None	Office of the Chief of Research and Development, Department of the Army

13. ABSTRACT

The scanning characteristics of a near-field Cassegrainian antenna excited with a relatively small planar array are investigated theoretically and experimentally. The analysis uses both geometrical optics and scalar diffraction theory. The technique is a viable approach to the problem of modifying an existing high-resolution dish radar for limited scan capability. Feed requirements can be satisfied by virtually any planar array concept, i.e., phase scanning, frequency scanning, multiple-beam-forming networks, etc. The scan range is roughly approximated by a fixed angular field of view; hence, the number of beamwidths scanned with electrically large apertures can be very high. Further, the system is free from the "coma" lobes usually associated with off-axis beams from a paraboloid. Design curves are presented from which one can determine the secondary characteristics - gain, scan loss, sidelobes, etc. - for a given array/reflector configuration.

14. KEY WORDS

electronic scanning
Cassegrainian antenna
planar array
beam-forming networks
reflectors
paraboloids

MASSACHUSETTS INSTITUTE OF TECHNOLOGY
LINCOLN LABORATORY

LIMITED ELECTRONIC SCANNING WITH A NEAR-FIELD CASSEGRAINIAN SYSTEM

W. D. FITZGERALD

Group 34

TECHNICAL REPORT 484

24 SEPTEMBER 1971

LEXINGTON MASSACHUSETTS

ABSTRACT

The scanning characteristics of a near-field Cassegrainian antenna excited with a relatively small planar array are investigated theoretically and experimentally. The analysis uses both geometrical optics and scalar diffraction theory. The technique is a viable approach to the problem of modifying an existing high-resolution dish radar for limited scan capability. Feed requirements can be satisfied by virtually any planar-array concept, i.e., phase scanning, frequency scanning, multiple-beam-forming networks, etc. The scan range is roughly approximated by a fixed angular field of view; hence, the number of beamwidths scanned with electrically large apertures can be very high. Further, the system is free from the "coma" lobes usually associated with off-axis beams from a paraboloid. Design curves are presented from which one can determine the secondary characteristics – gain, scan loss, sidelobes, etc.– for a given reflector configuration.

Accepted for the Air Force
Joseph R. Waterman, Lt. Col., USAF
Chief, Lincoln Laboratory Project Office

The work reported in this document was performed at Lincoln Laboratory, a center for research operated by Massachusetts Institute of Technology. The work is sponsored by the Office of the Chief of Research and Development, Department of the Army; it is supported by the Advanced Ballistic Missile Defense Agency and the Kwajalein Range Directorate, SAFSCOM under Air Force Contract F19628-70-C-0230.

CONTENTS

LIMITED ELECTRONIC SCANNING WITH A NEAR-FIELD CASSEGRAINIAN SYSTEM

I. INTRODUCTION

A typical phased-array antenna with electronic scan coverage encompassing a large fraction of a hemisphere can satisfy virtually any antenna system requirements. The obvious disadvantage of such systems is their high cost and complexity. On the other hand, fixed-beam antennas such as the steerable paraboloid have limited capabilities. Hybrid antenna systems, which combine mechanical and electronic beam steering, have application in systems which require rapid scan only over a limited angular region about the mechanical axis. A successful hybrid design would satisfy a radar's modest scan requirements by taking maximum advantage of the low cost and simplicity of a fixed-beam antenna and avoiding, to a large extent, the expense and complexity of a complete phased array. Instrumentation radars which must acquire and track a number of targets within a small angular sector are candidates for a hybrid system.

The measurements program for the BMD problem at the Western Test Range gave rise to the present study. A test mission generally involves a multiple-target complex restricted to an angular region much greater than the beamwidth of a system with sufficient sensitivity for measurements. Typically, the angular extent of the more interesting target complexes is 5° to 10°. The limitations of the fixed-beam radars exclude many interesting field experiments. A limited-scan hybrid system would simulate a complete high-resolution phased array over the angular region of interest. This would permit a wider range of more realistic field experiments for studying these "threat clouds" and associated data-processing problems.

A number of methods for providing a limited field of view have been investigated. Two basic approaches which use paraboloids are: (a) clusters of feed elements in either a focal point[1,2] or a Cassegrainian feed configuration,[3,4] and (b) array feeds – either conventionally fed or reflect arrays – which generally replace the subreflector in a Cassegrainian feed system.[5,6] The first approach has difficulties with "coma lobes," and for a high-power radar the switching matrix is a formidable problem. The latter has potentially a large field of view, but requires a large number of elements with a complex phase distribution. Complete arrays which use electrically large elements to reduce the number required have also been investigated for limited-scan applications.[7,8] These approaches use a random element separation to avoid the formation of grating lobes.

The limited field of view (LFOV) described here uses a near-field Cassegrainian antenna, which is excited by a small planar array operating in the near-field condition. The phase aberrations for off-axis beams are less with this system than with other paraboloidal feed configurations. When used with a high-resolution radar, this hybrid system has some attractive features in such areas as power-handling capability, freedom from "coma," efficiency, simplified beam

steering, reduced number of elements, etc. Our purpose is to present the performance characteristics of this system as determined by an analysis based on ray-tracing techniques and scalar diffraction theory, and to describe an experiment which was performed to verify the technique.

II. THE NEAR-FIELD CASSEGRAINIAN

Mercenne, a seventeenth-century friar, was the first to propose a reflecting telescope[9] which has become known to microwave antenna engineers as the near-field Cassegrainian (NFC) antenna.[10,11] A double-reflector system is used in which the main reflector and the subreflector are confocal paraboloids. The subreflector is illuminated with a linear phase front by placing it well into the near-field of a uniform phase feed aperture. For our purposes, the feed is a small electronically scanned planar array. The secondary beam is scanned simply by generating a linear phase front on the feed array. The optical analog is called an afocal telescope, which has collimated input and output wavefronts, the diameters of which differ by the magnification of the system. Linfoot[12] has shown that this system is free from third-order phase aberration. The coma lobe, usually encountered when one scans the pencil beam of a paraboloid off-axis, is caused principally by this third-order aberration term.

According to the laws of geometrical optics, maximum efficiency is achieved when the feed aperture has the same diameter as the subreflector and when the f/D (focal-length-to-diameter) ratios of the two reflectors are equal. When these conditions are satisfied, the main aperture is completely illuminated (except blockage, of course) without spillover. The feed array and subreflector have equal blocking when the outer edge of the array is in contact with the main reflector surface, i.e., when $d = d_{eff}$ in Fig. 1. This will be referred to as the minimum blockage condition. As the array is moved forward from the vertex toward the subreflector, the projection of the feed on the main aperture plane (or the effective blockage diameter) is increased as indicated in Fig. 1. The output wavefronts are collimated irrespective of the axial position of the array, i.e., the depth of focus is infinite. Also, it can readily be shown that there is no space attenuation with the NFC. A uniform distribution on the feed aperture yields a uniform distribution on the main aperture.

One can get a first impression of the mechanism involved in off-axis scanning by considering the near-field device to be the limiting case of a conventional Cassegrainian as the magnification becomes infinite. Figure 2 shows a conventional Cassegrainian system of large magnification,

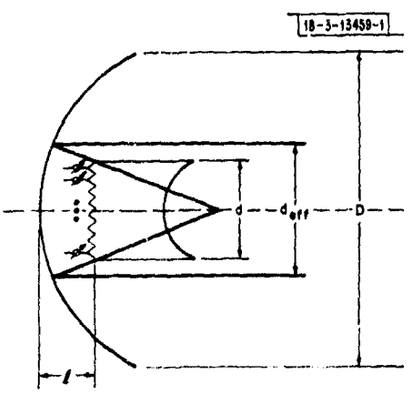

Fig. 1. Projected aperture-blocking characteristics with NFC geometry.

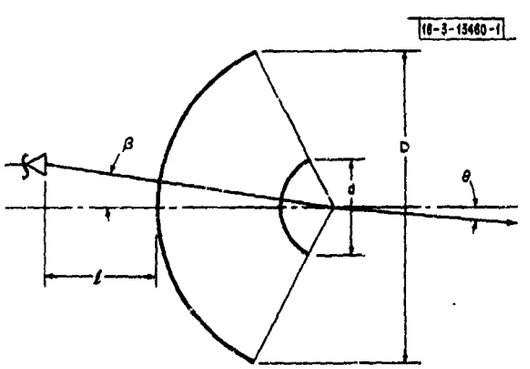

Fig. 2. Conventional Cassegrainian of high magnification.

in which the feed is laterally displaced by an amount Δ, which causes the secondary beam to be scanned off-boresight by the angle Θ. From the geometry, the angles Θ and β are related by $\tan\beta = (D/d)\tan\Theta$. As $f \to \infty$, the magnification becomes infinite and the hyperboloidal subreflector becomes a paraboloid. The feedhorn at $f = \infty$ can be replaced with a feed aperture (e.g., an array) of diameter d with a linear phase distribution, and positioned at or near the vertex of the main dish. To scan the secondary beam to an angle Θ, the array is required to generate a linear phase tilt β, where for small angles,

$$\beta \cong (D/d)\,\Theta \quad . \tag{1}$$

The simple astronomical telescope has similar characteristics. The lateral magnification (the ratio of focal lengths or D/d) is the reciprocal of the angular magnification Θ/β. Detailed analysis shows that Eq. (1) is accurate to within a negligibly small fraction of a beamwidth for all angles of scan within the system's capability.

In the near-zone region of a planar aperture, the fields are determined principally by geometrical propagation along the ray system. The radiated energy is contained within a column tilted from the array axis by the angle of scan β. Clearly, the spillover losses and the associated reduction in effective aperture will be a principal cause of scan loss.

III. ANALYSIS

Referring to Fig. 3, the ray-tracing analysis follows the path of a general ray from the plane of the array, through the dual-reflector system, to the main aperture plane. The coordinate points which describe the course of this ray through the reflector system are all normalized to unity, i.e., the coordinates describing the array and subreflector are normalized to d/2, and the coordinates of the main reflector and the main aperture plane are normalized to D/2. The angle β is the linear phase tilt assumed for the array. The x-z plane is taken as the plane of scan without loss in generality because of the circular symmetry of the system. The equation of the two reflectors (confocal paraboloids with the same f/d ratios) and Snell's Law at points of reflection are used to compute all the coordinate points required. The optical path length, $L = |AB| + |BC| + |CD|$, follows directly with all the coordinate points known. This ray-tracing analysis is described in detail in the Appendix.

For numerical analysis, the feed aperture is treated as a series of mesh points, as shown in Fig. 4. The coordinates $x_m = m/M$ and $y_n = m/M$ define a point on the array where $-M \leqslant m \leqslant M$ and $-M \leqslant n \leqslant M$. Coordinate points and optical path lengths are computed for all rays which originate on the feed aperture, i.e., for a given x_m, y_n assumes a set of values such that $-\sqrt{M^2 - m^2} \leqslant n \leqslant +\sqrt{M^2 - m^2}$ (closest integer). As x_m takes on all values between +1 and −1, all mesh points in the circular feed aperture are included.

The pattern $P(\Theta,\varphi)$ is computed using scalar diffraction theory. Thus,

$$P(\Theta,\varphi) = \sum_m \sum_n \Delta x'_{m,n}\Delta y'_{m,n} E'(x'_{m,n};y'_{m,n}) \times \exp\left[-j\Phi(x'_{m,n};y'_{m,n}) + jk_o(D/2)\sin\Theta\,(x'_{m,n}\cos\varphi + y'_{m,n}\sin\varphi)\right] \tag{2}$$

where Θ and φ are the spherical coordinates of a point in the far-field (see Fig. 5) and $k_o = 2\pi/\lambda$. This expression is based on the assumption that a continuous aperture can be represented by an array of "sampling" points, with the appropriate weighting factor. Each term of the summation represents one of these points and may also be viewed as the contribution from the "patch"

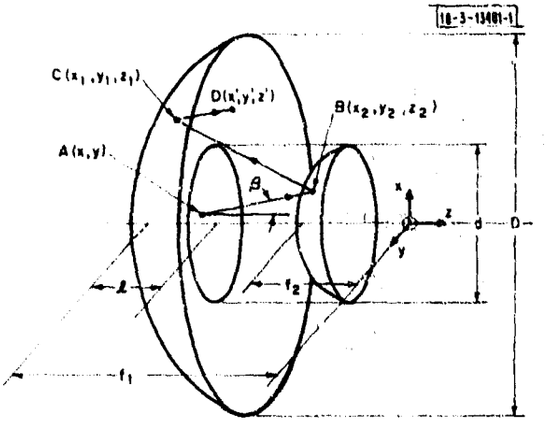

Fig. 3. Coordinates describing path of general ray through NFC system.

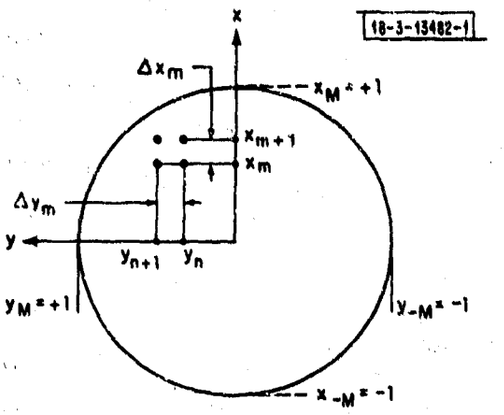

Fig. 4. Mesh points in feed aperture used for numerical analysis.

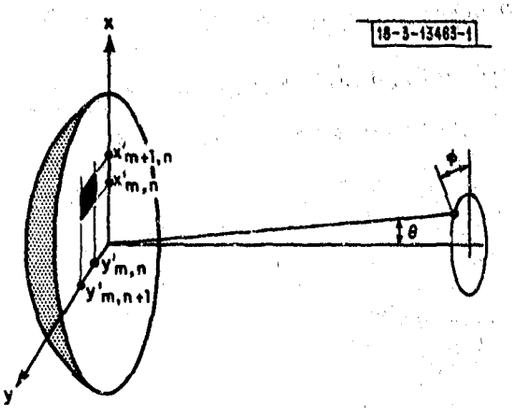

Fig. 5. Coordinate system and element of aperture used in pattern computations.

of aperture shown cross-hatched in Fig. 5 which is given by $\Delta x'_{m,n}\Delta y'_{m,n}$. The field strength over this elemental area is $E'(x'_{m,n};y'_{m,n})$.

The distribution $E'(x'_{m,n};y'_{m,n})$ is related to the assumed amplitude distribution on the array by power-flow considerations. A basic assumption in ray optics is that power flows along ray paths, hence the total energy flow within a tube bounded by a group of rays is constant even after successive reflections. This is written

$$\Delta x_m \Delta y_n E^2(x_m,y_n) = (D/d)^2 \Delta x'_{m,n}\Delta y'_{m,n} E'^2(x'_{m,n};y'_{m,n})$$

or

$$E'(x'_{m,n};y'_{m,n}) = (d/D) \frac{1}{M\sqrt{\Delta x'_{m,n}\Delta y'_{m,n}}} E(x_m,y_n) \tag{3}$$

where $E(x_m,y_n)$ is the electric-field distribution over the array aperture and $\Delta x_m = \Delta y_n = 1/M$. This expression assumes that the system is free from distortion, i.e., that an element of area on the main aperture, corresponding to a square element on the array aperture, is also square with the area given by $\Delta x_{m,n}\Delta y_{m,n}$. This assumption was investigated numerically, and we found that for a large amount of secondary-beam scan (5°), errors of 1 to 1½ percent occur at points in the vicinity of the diagonal planes. The integrated effect of this amount of diagonal-plane distortion may therefore be neglected.

The phase factor Φ in Eq. (2) is simply the sum of the electrical path length and the linear phase front assumed for the array

$$\Phi(x'_{m,n};y'_{m,n}) = k_o D \left[\frac{L_{m,n}}{D} + \frac{1}{2}\left(\frac{d}{D}\right) X_m \sin\beta\right] \quad . \tag{4}$$

By combining Eqs. (2), (3) and (4) and omitting unnecessary constants,

$$|P(\theta,\varphi)| = \left| \sum_m \sum_n \sqrt{\Delta x'_{m,n}\Delta y'_{m,n}}\, E(x_m,y_n) \exp\left\{-i\pi \frac{D}{\lambda}\left[2\,\frac{L_{m,n}}{D} + \left(\frac{d}{D}\right) x_m \sin\beta - \sin\theta\,(x'_{m,n}\cos\varphi + y'_{m,n}\sin\varphi)\right]\right\}\right| \quad . \tag{5}$$

The plane of scan is the plane $\varphi = 0$. This expression must be evaluated in order to (a) exclude rays which are "spilled over" the subdish or the main dish and (b) take account of the aperture blockage caused by the subreflector and feed. These requirements are satisfied if the summation is taken over values of m and n for which

$$\left(\frac{d_{eff}}{D}\right)^2 \leq x'^2_{m,n} + y'^2_{m,n} \leq 1 \quad .$$

The quantity d_{eff} is the projected blockage diameter as indicated in Fig. 1.

To compute the patterns over a large angular sector, the point separation would have to approach $\lambda/2$. This presents an excessive computational load when dealing with apertures which are hundreds of wavelengths in extent. The number of required points, however, is dramatically reduced if we restrict the region of interest to the principal lobe and the first few sidelobes adjacent to the principal lobe. (The off-axis patterns correspond to an approximate linear phase constant across the points, and hence are of little significance in determining the number of

points required.) Allen[13] has shown that the accuracy of these computations over the angular sector Θ_{max} is determined by the factor $(\Theta_{max}/M)(D/\lambda)$. We found that for M = 20 (approximately 1200 points in the aperture) the maximum error over the first three sidelobes was less than 1.0 dB. Although not optimum from the point of view of computer economy, the value M = 20 was used in Eq. (5) since it represents a manageable computational load with negligible quantization errors.

The aperture efficiency of the boresight beam is given by

$$\eta \quad \frac{\left| \sum_m \sum_n E(x_m, y_n) \right|^2}{M^2 \sum_m \sum_n |E(x_m, y_n)|^2}$$

where the numerator is summed over values of m and n for which

$$\left(\frac{d_{eff}}{D}\right)^2 \leq x_m^2 + y_n^2 \leq 1 \tag{7}$$

and the denominator is summed over values of m and n for which $0 \leq x_m^2 + y_n^2 \leq 1$. The computed efficiency includes blockage loss and the amplitude taper efficiency. There are no spillover losses for the boresight beam in the ray-optics description of the system.

Equations (5) and (6) are sufficient for evaluation of all the secondary characteristics of interest. Aperture efficiency is computed for $\beta = 0$, and patterns are computed for six values of β from $\beta = 0°$ to 15° in 3° increments. The peak values of the off-axis patterns are normalized to the boresight values. There are five input parameters to the computer program:

d/D	the ratio of subreflector diameter to main-reflector diameter
f/D	the focal-length-to-diameter ratio; this parameter is the same for both reflectors
D/λ	the diameter of the main reflector in wavelengths
ℓ/f_1	the distance from the array aperture to the vertex of the main reflector normalized to the focal length of the main reflector
$E(x_m, y_n)$	the assumed electric-field distribution on the array aperture.

The computations are performed with the array diameter always equal to the subreflector diameter. This corresponds to the optimum illumination condition mentioned earlier.

IV. COMPUTED RESULTS

If each of the five input parameters is varied over its interesting range, the number of computed patterns quickly runs into the thousands. Our problem is to reduce this large quantity of data into useful design curves from which one can determine scan loss, efficiency, sidelobes, beamwidth, etc., for a given set of input parameters.

We consider first the significance of the parameter ℓ/f. The distance from the array face to the vertex of the main reflector for the minimum blocking condition ($d = d_{eff}$) is designated $\ell = \ell_{min}$ where

$$\frac{\ell_{min}}{f_1} = \frac{(d/D)^2}{(4f/D)^2} \tag{8}$$

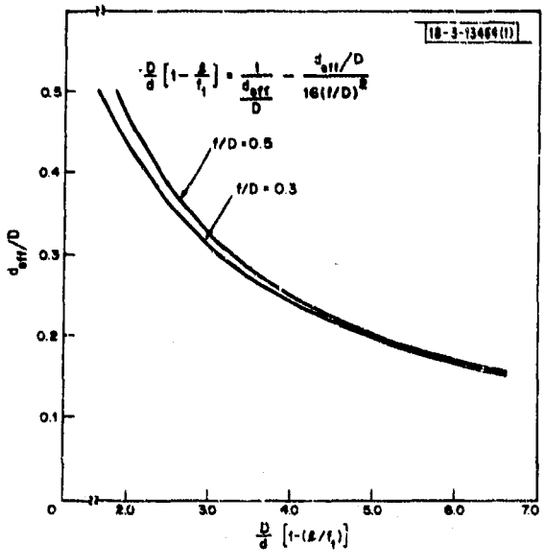

Fig. 6. Effective blockage ratio as function of geometrical parameters.

If we increase ℓ and decrease d so as to keep d_{eff} constant, then for a given β the form of the patterns (scan loss, beamwidth, sidelobes, etc.) is invariant.. The angle of scan, however, is reduced by the factor d/d_{eff}. Figure 6 shows the relationship between d_{eff}/D and the quantity $(D/d)\,[1-(\ell/f_1)]$. The computed patterns of Figs. 7(a-b) and 8 illustrate the effect of maintaining a constant effective blockage diameter. For both sets of patterns, $d_{eff}/D = 0.3$. For the patterns of Fig. 7(a), $d_{eff} = d$, hence $d/D = 0.3$. The patterns of Fig. 7(b) are for the case $d/D = 0.2$ and $d/d_{eff} = 0.667$. For any value of β, the corresponding patterns of Figs. 7(a) and (b) are identical, but the angle of scan in Fig. 7(b) is reduced by the factor d/d_{eff}. Mathematically, if the pattern in the plane of scan ($\varphi = 0$) for $d = d_{eff}$ is given by $P(\Theta - \Theta_o; \varphi)$, then

$$P(\Theta - \Theta_o; 0) = P\left(\Theta - \frac{d}{d_{eff}}\Theta_o; 0\right) \tag{9}$$

providing d_{eff} is constant. The beam position Θ_o is given by Eq. (1). With the curves of Fig. 6 and Eq. (9), the secondary characteristics can be completely determined for any ℓ from calculations for the case $\ell = \ell_{min}$ only. This "elimination" of one of the five input parameters simplifies the problem of data reduction. Subsequent curves describing performance characteristics do not explicity involve ℓ/f_1.

A. Boresight Characteristics

Figure 8 shows the aperture efficiency and the sidelobe characteristics as a function of the effective blocking ratio for the boresight beam. The amplitude distributions used with Eqs. (5) and (6) are

$$E(x_m, y_n) = [1 - (x_m^2 + y_n^2)]^K + C \tag{10}$$

The constants K and C control, respectively, the form of the taper and the edge illumination. We will be principally concerned with two sets of constants: K = 1 and C = 0, which is the familiar

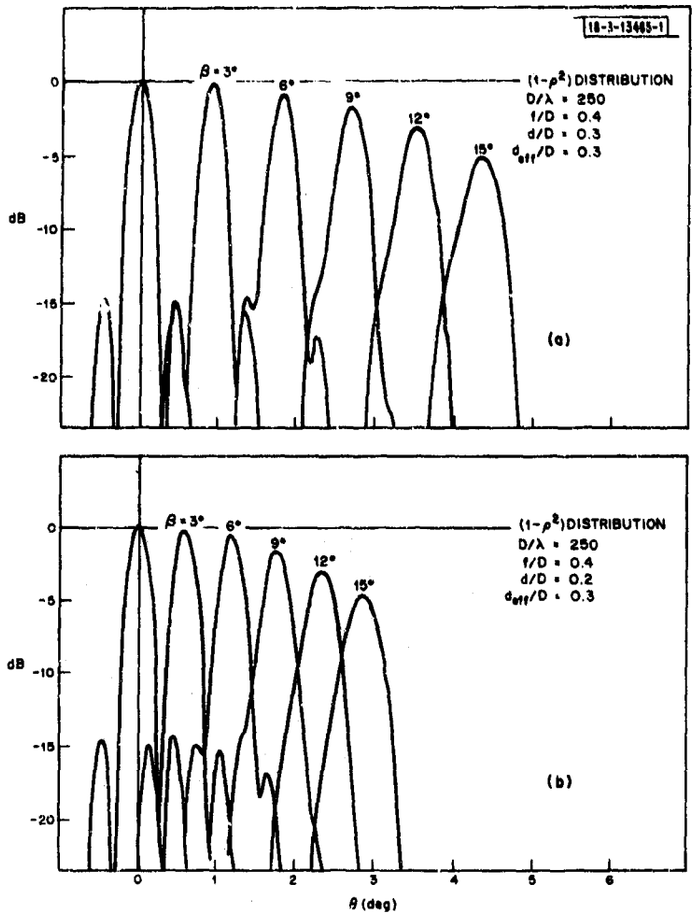

Fig. 7(a-b). Computed patterns showing behavior with d_{eff}/D constant.

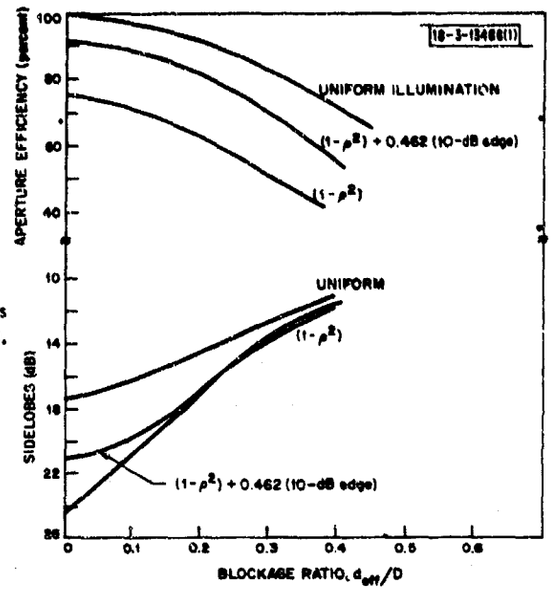

Fig. 8. Efficiency and sidelobe characteristics of circular aperture with blockage ratio d_{eff}/D.

$(1-\rho^2)$ distribution; and with K = 0 and C = 0, the uniform distribution. Figure 8 also includes a tapered distribution with a 10-dB edge illumination. The high aperture efficiencies for the uniform illumination reflect the fact that the NFC geometry does not have space attenuation. The curves show the penalty paid in terms of reduced efficiency and increased sidelobe levels when large effective blockage ratios are used. Unfortunately, a large field of view is accompanied by a large blockage ratio. The sidelobes are computed for the boresight condition, but because of the absence of coma, the levels shown represent (for all practical purposes) the maximum levels encountered for any off-axis beam.

The curves of Fig. 8 apply generally to a circular aperture with central blockage given by d_{eff}/D and with the distributions as indicated.

B. Off-Axis Characteristics

As mentioned earlier, the scan range which can be achieved with this system is limited principally by spillover (in both forward and reverse directions) and the accompanying reduction in effective aperture. If this were the only cause of scan loss, the system would have a fixed angular field of view, independent of frequency. Scan loss, of course, is also caused by phase aberrations and, to a lesser extent, by amplitude dispersion.

Figures 9 and 10 show typical normalized path-length errors across a central strip of the main aperture in the plane of scan. A small linear component, which represents the error in Eq. (1), has been removed. This error is a negligibly small fraction of a beamwidth for all cases of interest. The dashed line is indicative of the amount by which the effective aperture is reduced in this central strip. Deeper dishes and larger subreflectors (Fig. 10) have less aperture reduction but greater path-length errors. The aperture sizes for which the path-length errors represent a maximum phase error ($\Delta\varphi$) of $\pi/2$ are as indicated. The value of $\pi/2$ is somewhat arbitrarily chosen as the amount of error which produces noticeable degradation of the patterns. The amplitude variation, i.e., the dispersion or space attenuation for off-axis beams, across this central strip was not found to be of great significance. For example, by using the parameters

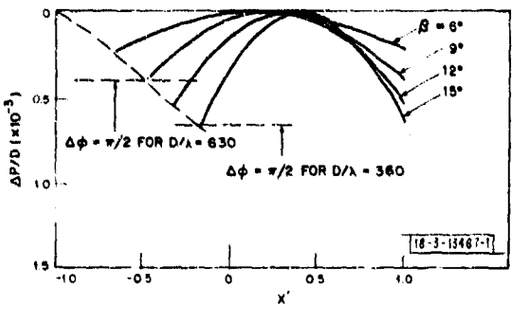

Fig. 9. Path-length errors in central aperture strip for f/D = 0.4, d/D = 0.25, d = d_{eff}.

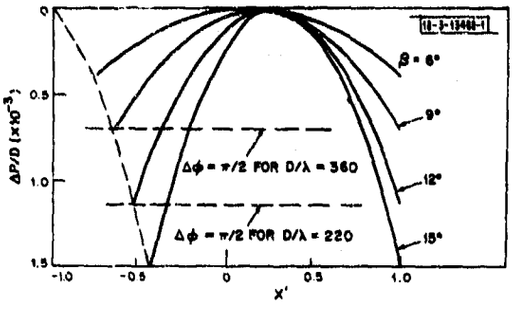

Fig. 10. Path-length errors in central aperture strip for f/D = 0.3, d/D = 0.3, d = d_{eff}.

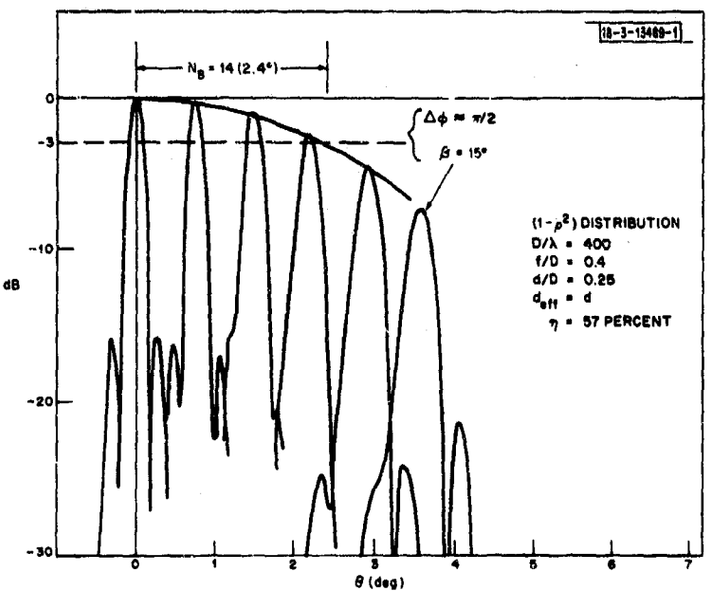

Fig. 11. Computed patterns with path-length errors corresponding to Fig. 9.

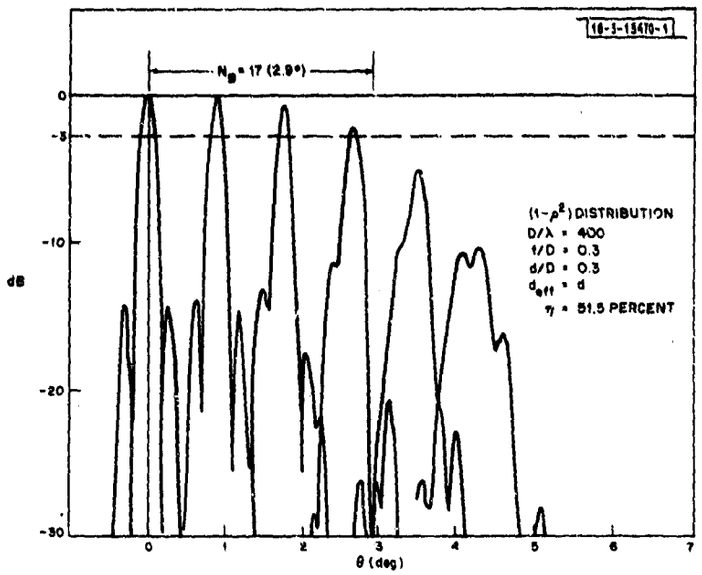

Fig. 12. Computed patterns with path-length errors corresponding to Fig. 10.

of Fig. 9, the amplitude variation across the effective aperture for $\beta = 15°$ is approximately linear and less than 2 dB.

Figure 11 shows the computed patterns with the geometrical parameters of Fig. 9 and with an aperture of 400 wavelengths. In this example, $\Delta\varphi$ is approximately $\pi/2$ for the beam which corresponds to $\beta = 15°$. Note the absence of coma. The sidelobes are maximum on boresight and the beam is well-defined and usable well beyond the −3-dB scan-loss point. The patterns corresponding to the path-length errors of Fig. 10 with an aperture diameter of 400 wavelengths are shown in Fig. 12 which is a more extreme example in which phase errors play a substantial role in limiting scan range and degrading patterns. The maximum phase error is $\pi/2$ at approximately the 2-dB scan-loss point. A larger f/D in this example would markedly improve performance.

We found that the large amount of data can be reduced to useful curves which summarize scanning characteristics if the appropriate quantities are plotted. These curves are shown in Figs. 13 and 14 for the two distributions considered. The quantity N_B in these curves is the number of half-power beamwidths scanned from boresight to the −3-dB scan-loss point. The total field of view as defined by the −3-dB scan-loss criterion is then $2N_B$ beamwidths. The range of parameters used in computing these curves is: $0.1 \leqslant d_{eff}/D \leqslant 0.35$, and $68 \leqslant D/\lambda \leqslant 400$, with the f/D's as indicated. Note that the curves are based on the effective blocking ratio d_{eff}/D. Figure 6 and Eq. (9) can be used to include the more general case where $d \neq d_{eff}$. This is useful if one wishes to trade off scan range for reduced array size (a linear trade).

Some observations on these summary curves and on the secondary characteristics in general follow:

> These curves would be linear if the system had a fixed angular field of view as predicted by the simple model which neglects phase errors. Note that the linear approximation is quite good over an appreciable range for the larger f/D's.

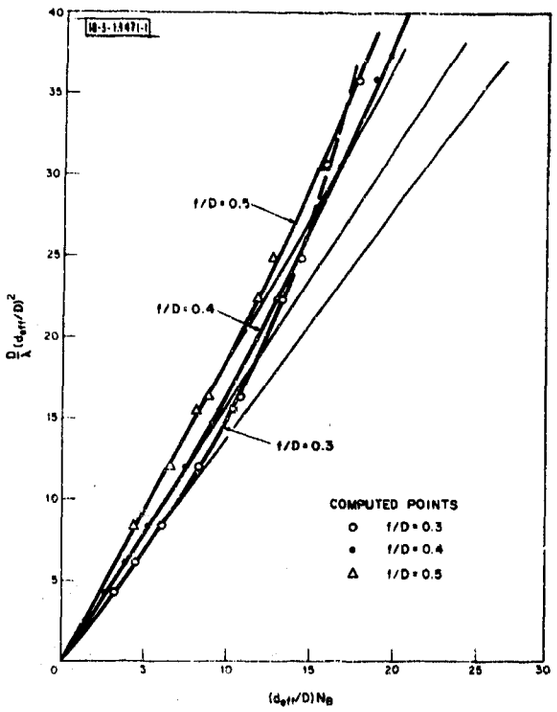

Fig. 13. Scan summary curves with $(1-\rho^2)$ distribution. N_B is number of half-power beamwidths scanned from boresight to −3-dB scan-loss point.

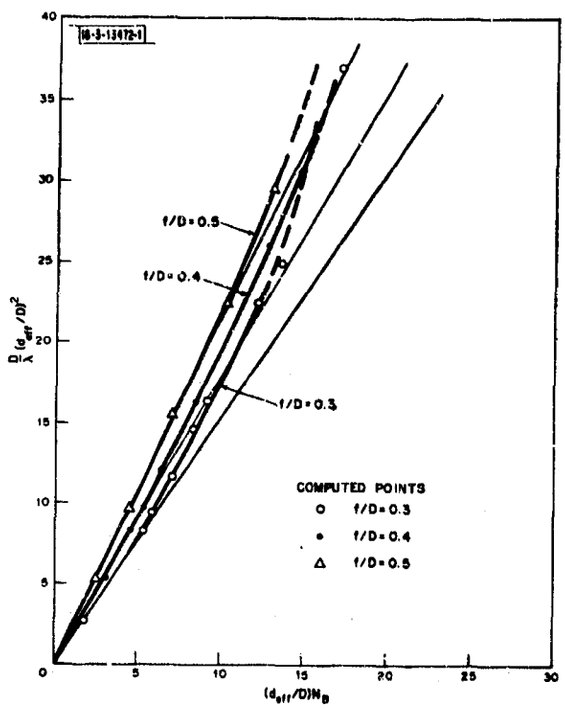

Fig. 14. Scan summary curves with uniform distribution. N_B is number of half-power beamwidths scanned from boresight to −3-dB scan-loss point.

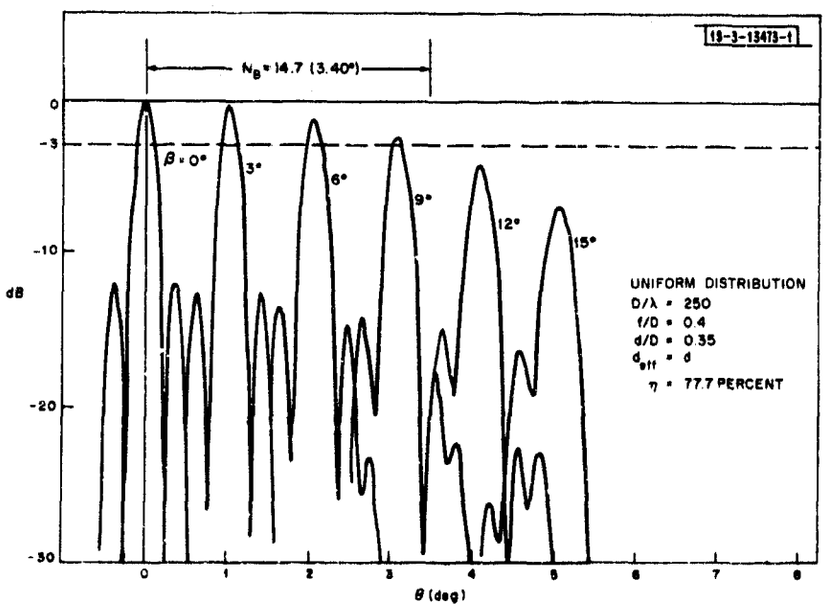

Fig. 15. Computed patterns with uniform distribution.

There is no problem with coma lobes. For any set of design parameters of interest, the off-axis sidelobes are approximately equal to, or less than, the boresight sidelobes. Figures 7(a) and (b) and 11 are typical examples.

The beam broadening with −3-dB scan loss is approximately 50 percent for both distributions.

Deeper dishes are to be preferred for low-to-moderate values of N_B. This is perhaps the most interesting range of application.

Figures 15 and 16 show the computed patterns for a large blockage ratio $d_{eff}/D = 0.35$, with $f/D = 0.4$ and $D/\lambda = 250$. Note that the difference in boresight efficiency between the uniform (Fig. 15) and the tapered (Fig. 16) distributions is 2.4 dB. The sidelobes are not appreciably different. Based on the average gain over a given scan range, the uniform illumination is clearly superior.

For a fixed D/λ and a fixed array size, scan range is increased as the array is brought closer to the subreflector. This is accompanied by the reduced efficiency and the higher sidelobes associated with the larger d_{eff}/D.

Hogg and Semplak[10] measured good patterns and efficiencies with a near-field Cassegrainian antenna in which the subreflector was as far as $1/15$ $(2d^2/\lambda)$ from the feed. This separation is equivalent to $N_B \cong 2$ on our curves. Hence, if $N_B \cong 2$, the near-field condition is satisfied.

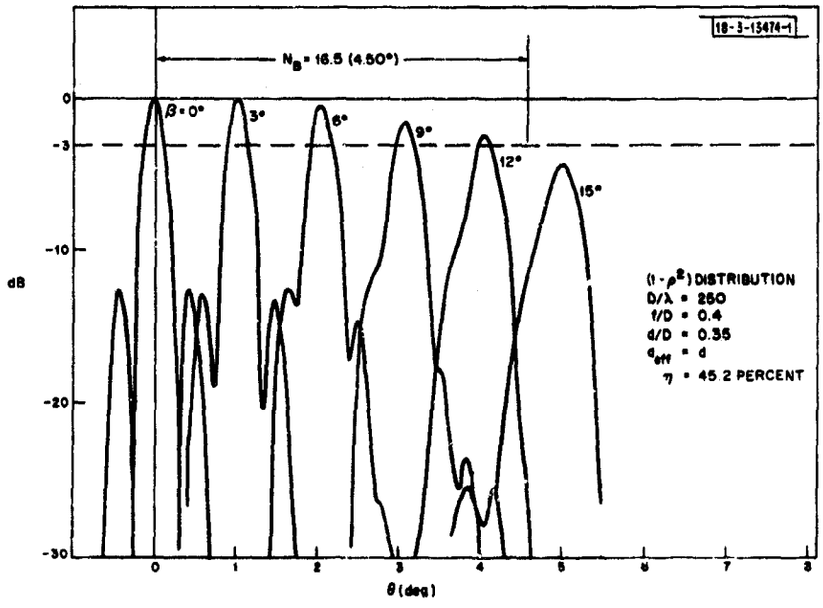

Fig. 16. Computed patterns with $(1-\rho^2)$ distribution.

Fig. 17. Photograph of equipment used in experiment.

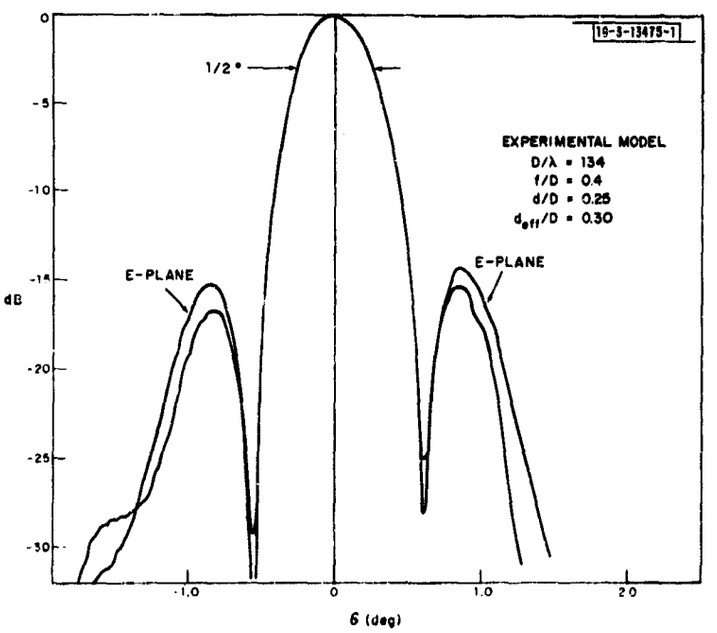

Fig. 18. Measured principal-plane boresight patterns.

V. EXPERIMENTAL DEMONSTRATION

An experiment was performed with the equipment shown in Fig. 17. For convenience, the array is simulated by a paraboloid with a point source feed which was designed to enable the feed dish to be rotated about an axis in its aperture plane. The main reflector is a precision 6-foot paraboloid, and the frequency used in the experiment was 22.0 GHz. Figure 18 shows the measured boresight patterns in the principal planes, and Fig. 19(a-b) shows a comparison between measured and computed scan characteristics. The agreement between theory and experiment is good. The slight differences observed are the result of:

(a) The effective aperture of an electronically scanned array decreases with $\cos\beta$. Consequently, a mechanically rotated aperture would involve less spillover and therefore a slight increase in secondary scan.

(b) The fact that the feed-dish aperture has a more pronounced taper than the $(1 - \rho^2)$ distribution used in the calculations.

Patterns were also measured in the plane orthogonal to the plane of scan to demonstrate that the effects of astigmatism are negligible. For the beam with −3-dB scan loss, the orthogonal plane patterns have a negligible change in beamwidth (< 5 percent) and the increase in sidelobes is < 1 dB.

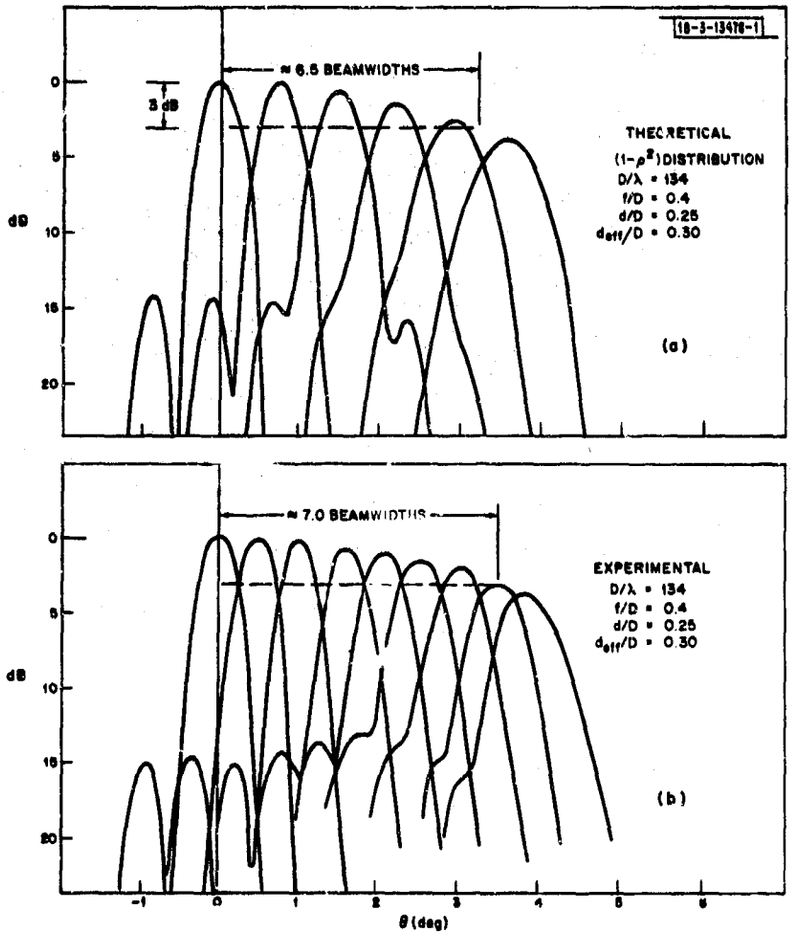

Fig. 19. Comparison of (a) theoretical and (b) experimental scan characteristics.

VI. FEED CONSIDERATIONS

The feed requirements for this LFOV system can be satisfied by any conventional planar array. Phase scanning, frequency scanning, and even multiple-beam-forming techniques are applicable. A Butler matrix, for example, which forms N independent simultaneous beams with nominal crossover levels of 3 dB, will form the same number of secondary beams with approximately the same crossover levels, except at the extremes of scan where the levels are reduced somewhat due to beam broadening. The constant angular magnification [Eq. (1)] preserves the relative positions of primary and secondary beams.

The number of elements required by the array can be reduced substantially by virtue of the limited scan required, and by the inherent suppression of grating lobes with the near-field Cassegrainian geometry. This occurs because the grating lobes appear at large angles from the array boresight. As a result, the grating-lobe energy is not intercepted by the subreflector, whereas the energy associated with the main beam is magnified by the optics of the system, i.e., approximately $(D/d)^2$. If the elements are electrically large (area-type elements with the area $\sim\lambda^2$), the additional scan loss incurred follows the form of the element factor. For example, if $\beta_{max} = 12°$, a square element 1.25λ on a side results in an increased scan loss at β_{max} of less than 1.0 dB. This assumes a uniform distribution over the array element. The grating-lobe level in the secondary depends on the parameters of the reflector system, but it is typically −20 dB. For most applications, the number of elements can be reduced by a factor of 4 to 6 as compared with the case where the element separation is $\lambda/2$. Note that this is accomplished with periodic spacing of the elements. Hence, the desirable row-column beam-steering technique is still applicable.

An obvious approach to the design of an array for this application would use contiguous square-horn radiators. Unfortunately, a simple horn with an $a/\lambda > 1.0$ has an aperture efficiency of only 81 percent. A technique was developed[14] to control the field distribution in the aperture

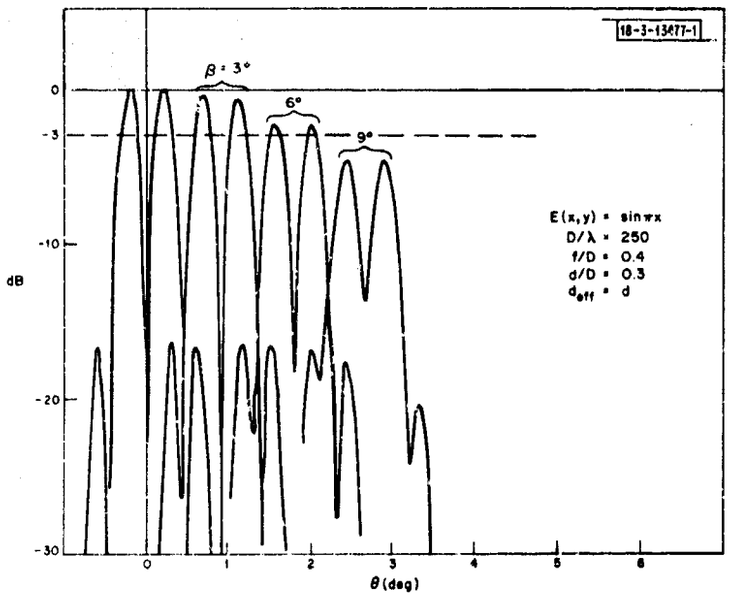

Fig. 20. Scanned error patterns for full-wave sine-difference distribution.

of this simple horn with the use of dielectric wedges, and thereby increase its efficiency. It has been demonstrated that efficiencies of 93 to 96 percent can be realized with bandwidths of approximately 15 percent. An array constructed with these more efficient horns reduces the 1.0-dB loss (which is the energy lost in the H-plane grating lobes) to approximately 0.25 dB.

Figure 20 is an example of the behavior of the scanned difference patterns. The distribution chosen is a full-wave sinusoid, i.e., $E(x_m, y_n) = \sin \pi x_m$. The scan loss is greater than that of the sum patterns with the same parameters [Fig. 7(a)], and the null depth is appreciably reduced at the extremes of scan. This is not surprising, considering that we have a substantial amount of spillover on only one side of an odd aperture distribution. The situation can be improved by using only a portion of the array aperture to generate the error patterns. This would, in effect, trade off boresight-tracking efficiency for improved off-axis performance. A multiple-beam-forming matrix which forms synthetic difference patterns would avoid this problem.

VII. CONCLUSIONS

The dual-reflector system described is a very practical approach to the design of an LFOV system. If the system requirements are compatible with the limited range of electronic scan afforded, the LFOV system combines the high resolution and (to a large degree) the low cost of a reflector antenna with the versatility and flexibility of continuous electronic scanning. Design curves are presented which enable the determination of the performance levels and tradeoffs between scan range, array size, efficiency, sidelobes, etc., for all interesting ranges of system parameters. Some advantages of this LFOV technique worthy of mention are:

The feed array utilizes linear phase scanning. Hence, virtually any planar array concept – phase scanning, frequency scanning, multiple-beam-forming networks, etc. – is suitable for use as a feed.

The restricted range through which the array is required to scan and the inherent grating-lobe discrimination of the optical system permit the number of elements (and consequently the cost) to be considerably reduced while maintaining uniform element separation.

The "coma" lobes, characteristic of off-axis beams from a paraboloid, are avoided with this system.

The scan range can be roughly approximated by a fixed angular field of view. Consequently, the number of beamwidths scanned for electrically large apertures can be very high.

The main disadvantage of the system is the deleterious effects on efficiency and sidelobes resulting from the relatively large amounts of blockage required for good scan range.

The diffraction effects introduced by both the near-field assumption and the edge effects associated with the reflectors have not been considered. The analysis is subject to this limitation.

ACKNOWLEDGMENT

The author wishes to thank Mr. Carl Blake and Dr. G.N. Tsandoulas for encouragement and helpful discussions, Miss Susan A. Rejunas for writing the computer program, and Mr. E. F. Pelrine for assistance with the measurements effort.

REFERENCES

1. K.S. Kelleher and H.P. Coleman, "Off Axis Characteristics of the Paraboloidal Reflector," Naval Research Laboratory Report 4088 (1952).
2. J. Ruze, "Lateral-Feed Displacement in a Paraboloid," IEEE Trans. Antennas Propag. AP-13, 660-665 (1965), DDC AD-625018.
3. J. Nihen and A. Kay, "Optimum Dual Reflector Antenna Design Investigation," Technical Report RADC-TOR-63-318 (June 1963).
4. "Investigation of Multifeed Antennas and Wide Angle Optics," Airborne Instruments Laboratory (January 1960).
5. C. F. Winter, "Phase-Scanning Experiments with Two-Reflector Antenna Systems," Proc. IEEE 56, 1984-1999 (1968).
6. D.G. Berry, R.G. Malech and W.A. Kennedy, "The Reflectarray Antenna," Trans. IEEE, PTGAP AP-11, 645-651 (1963).
7. W.T. Patton, "Analysis of Radar Electronic Scan Technique," Technical Report, ESD-TR-66-335, SEDCO Systems Inc., Farmingdale, New York (July 1966).
8. L. Mansky, L. Simpson and M. Simpson, "A Development Study of Technique to add Electronic Scanning and Multiple-Target Tracking to a Fixed Beam Radar," Final Report, ESD-TR-66-300, SEDCO Systems Inc., Farmingdale, New York (July 1966).
9. H.C. King, The History of the Telescope (Sky Publishing Corporation, Cambridge, Massachusetts, 1955).
10. D.C. Hogg and R.A. Semplak, "An Experimental Study of Near-Field Cassegrainian Antennas," Bell System Tech. J. 43, 2677-2704 (1964).
11. S.P. Morgan, "Some Examples of Generalized Cassegrainian and Gregorian Antennas," Trans. IEEE, PGAP AP-12, 685-691 (1964).
12. E.H. Linfoot, Recent Advances in Optics (Oxford University Press, Amen House, London, 1955).
13. C.C. Allen, "Numerical Integration Methods for Antenna Pattern Calculations," Trans. IRE, PGAP AP-7 Suppl., S387-S401 (1959).
14. G.N. Tsandoulas and W.D. Fitzgerald, "Aperture Efficiency Enhancement in Dielectrically Loaded Horns," IEEE Trans. Antennas Propag. (to be published).

APPENDIX
RAY-TRACING ANALYSIS

Referring to Fig. 3, we compute the path length of a general ray from a point (x, y) on the array aperture through the two-reflector system to a point in the aperture plane (x', y'). The origin coincides with the focal point of both paraboloids and the array is scanned only in the x-z plane. A point on the subreflector is denoted by (x_2, y_2, z_2). Similarly, (x_1, y_1, z_1) defines a point on the main reflector.

The general ray emerging from the array aperture is perpendicular to the assumed linear phase front β and hence is parallel to

$$\overline{ab} = \bar{i} \sin\beta + \bar{k} \cos\beta \quad . \tag{A-1}$$

Lower-case letters denote unit vectors, and $\bar{i}$, $\bar{j}$, $\bar{k}$ are the unit vectors along the coordinate axes. The unit vector along the component path length AB is

$$\frac{\overline{AB}}{|AB|} = \frac{\bar{i}(x_2 - x) + \bar{k}(z_2 + f_1 - \ell)}{\sqrt{(x_2 - x)^2 + (z_2 + f_1 - \ell)^2}} \quad . \tag{A-2}$$

Equating components of Eqs. (A-1) and (A-2) yields a single independent equation:

$$\tan\beta = \frac{x_2 - x}{z_2 + f_1 - \ell} \tag{A-3}$$

which, when combined with the equation of the subreflector

$$z_2 = \frac{x_2^2 + y_2^2}{4f_2} - f_2 \tag{A-4}$$

gives the coordinates of the first point of reflection B:

$$x_2 = \frac{2f_2}{\tan\beta} - 2\left[(f_2/\tan\beta)^2 - f_2\left(\frac{x}{\tan\beta} + \frac{y^2}{4f_2} + f_1 - f_2 - \ell\right)\right]^{1/2}$$

$$y_2 = y \quad . \tag{A-5}$$

Snell's law of reflection applied to this point on the subreflector is expressed as

$$\overline{bc} = \overline{ab} - 2\bar{n}_2(\bar{n}_2 \cdot \overline{ab}) \tag{A-6}$$

where $\overline{bc}$ is along the reflected ray, and $\bar{n}_2$ is the outward-directed unit normal given by

$$\bar{n}_2 = \frac{\bar{i}_1 x_2 + \bar{j} y_2 - \bar{k}(2f_2)}{\sqrt{x_2^2 + y_2^2 + (2f_2)^2}} \quad . \tag{A-7}$$

By using Eqs. (A-1) and (A-7) in Eq. (A-6),

$$\overline{bc} = \bar{i}(bc)_x + \bar{j}(bc)_y + \bar{k}(bc)_z$$

$$= \bar{i}\left[\sin\beta - \frac{2x_2(x_2\sin\beta - 2f_2\cos\beta}{x_2^2 + y_2^2 + 4f_2^2}\right] + \bar{j}\left[\frac{-2y_2(x_2\sin\beta - 2f_2\cos\beta)}{x_2^2 + y_2^2 + 4f_2^2}\right]$$

$$+ \bar{k}\left[\cos\beta + \frac{4f_2(x_2\sin\beta - 2f_2\cos\beta)}{x_2^2 + y_2^2 + 4f_2^2}\right] \quad . \tag{A-8}$$

Proceeding as before, the unit vector $\overline{bc}$ is expressed in terms of the coordinates of the points B and C

$$\overline{bc} = \frac{\overline{BC}}{|\overline{BC}|} = \frac{\bar{i}(x_1 - x_2) + \bar{j}(y_1 - y_2) + \bar{k}(z_1 - z_2)}{\sqrt{(x_1 - x_2)^2 + (y_1 - y_2)^2 + (z_1 - z_2)^2}} \quad . \tag{A-9}$$

Equating components of Eqs. (A-8) and (A-9), we have three equations which describe a line in space. Only two of these equations are independent. Thus,

$$\frac{(bc)_x}{(bc)_y} = \frac{y_1 - y_2}{x_1 - x_2}$$

$$\frac{(bc)_z}{(bc)_y} = \frac{z_1 - z_2}{y_1 - y_2} \tag{A-10}$$

All quantities except the coordinates of point C (x_1, y_1, z_1) are taken as constants. Combining Eqs. (A-10) with the equation of the main reflector

$$z_1 = \frac{x_1^2 + y_1^2}{4f_1} - f_1 \tag{A-11}$$

yields the coordinates of the second point of reflection C:

$$y_1 = \frac{-F \pm \sqrt{F^2 - 4EG}}{2E}$$

$$x_1 = x_2 + \frac{(bc)_x}{(bc)_y}(y_1 - y_2) \tag{A-12}$$

where

$$E = 1 + \left[\frac{(bc)_x}{(bc)_y}\right]^2$$

$$F = 2\frac{(bc)_x}{(bc)_y}x_2 - 2\left[\frac{(bc)_x}{(bc)_y}\right]^2 y_2 - 4f_1\frac{(bc)_z}{(bc)_y}$$

$$G = 4f_1(f_2 - f_1) + \left(1 - \frac{f_1}{f_2}\right)x_2^2 + \left\{\left[\frac{(bc)_x}{(bc)_y}\right]^2 - \frac{f_1}{f_2}\right\}y_2^2$$

$$+ 4f_1\frac{(bc)_z}{(bc)_y}y_2 - 2\frac{(bc)_x}{(bc)_y}x_2y_2 \quad .$$

Again, using Snell's law at the point of reflection on the main reflector,

$$\overline{cd} = \overline{bc} - 2\bar{n}_1(\bar{n}_1 \cdot \overline{bc}) \quad . \tag{A-13}$$

The unit normal on the main reflector is

$$\bar{n}_1 = \frac{-\bar{i}x_1 - \bar{j}y_1 + \bar{k}(2f_1)}{\sqrt{x_1^2 + y_1^2 + 4f_1^2}} \quad . \tag{A-14}$$

By using Eqs. (A-8) and (A-14) in Eq. (A-13),

$$\begin{aligned}\overline{cd} &= \bar{i}(cd)_x + \bar{j}(cd)_y + \bar{k}(cd)_z \\ &= \bar{i}\left\{(bc)_x + \frac{2x_1\,[-x_1(bc)_x - y_1(bc)_y + 2f_1(bc)_z]}{x_1^2 + y_1^2 + 4f_1^2}\right\} \\ &\quad + \bar{j}\left\{(bc)_y + \frac{2y_1\,[-x_1(bc)_x - y_1(bc)_y + 2f_1(bc)_z]}{x_1^2 + y_1^2 + 4f_1^2}\right\} \\ &\quad + \bar{k}\left\{(bc)_z - \frac{4f_1\,[-x_1(bc)_x - y_1(bc)_y + 2f_1(bc)_z]}{x_1^2 + y_1^2 + 4f_1^2}\right\} \quad .\end{aligned} \tag{A-15}$$

Equating the components of Eq. (A-15) with

$$\frac{\overline{CD}}{|\overline{CD}|} = \frac{\bar{i}(x' - x_1) + \bar{j}(y' - y_1) + \bar{k}(z' - z_1)}{\sqrt{(x' - x_1)^2 + (y' - y_1)^2 + (z' - z_1)^2}} \tag{A-16}$$

again yields two independent equations:

$$\begin{aligned}\frac{(cd)_x}{(cd)_y} &= \frac{x' - x_1}{y' - y_1} \\ \frac{(cd)_x}{(cd)_z} &= \frac{x' - x_1}{z' - z_1} \quad .\end{aligned} \tag{A-17}$$

The aperture plane is defined by

$$z' = \frac{D^2}{16f_1} - f_1 \quad . \tag{A-18}$$

Combining Eqs. (A-17) and (A-18) gives the coordinates of the point in the aperture plane D:

$$\begin{aligned}x' &= x_1 + \frac{(cd)_x}{(cd)_z}\left(\frac{D^2}{16f_1} - f_1 - z_1\right) \\ y' &= y_1 + \frac{(cd)_y}{(cd)_x}(x' - x_1) \quad .\end{aligned} \tag{A-19}$$

The total path length of the general ray is

$$L = |AB| + |BC| + |CD|$$

$$= \sqrt{(x_2 - x)^2 + (z_2 + f_1 - \ell)^2} + \sqrt{(x_1 - x_2)^2 + (y_1 - y_2)^2 + (z_1 - z_2)^2}$$

$$+ \sqrt{(x' - x_1)^2 + (y' - y_1)^2 + (z' - z_1)^2} \quad . \qquad \text{(A-20)}$$

For use with the computer program, all coordinates are normalized as follows:

$$x,\ y,\ \ell,\ x_2,\ y_2,\ z_2 \quad \rightarrow \quad d/2$$

$$x_1,\ y_1,\ z_1,\ x',\ y',\ z' \quad \rightarrow \quad D/2 \quad .$$

The "constant" inputs to the ray-tracing portion of the program are f/D, d/D, ℓ/f_1, and the angle of scan β. For an assumed pair of feed aperture coordinates (x, y), the coordinates of all points of reflection which define the passage of the ray through the system are computed and then used to compute the optical path length given by Eq. (A-20).

It is of interest to note that the basic properties of the NFC can readily be shown with these equations. For the case $\beta = 0$, Eq. (A-20) reduces to

$$L/D = (2f/D)\left(1 - \frac{d}{D}\right) - (f/D)\,(\ell/f_1) + \frac{1}{16(f/D)}$$

which is independent of the coordinates defining the array or the main aperture. This proves the collimating property of the NFC. Also, for the case $\beta = 0$, Eq. (A-19) reduces to

$$x' = (D/d)\,x$$

$$y' = (D/d)\,y \quad .$$

Hence, $dx'/dx = dy'/dy = \text{constant}$. This proves that the NFC does not have space attenuation.